Role of Ionic Interactions in Ligand Binding and Catalysis of R67 Dihydrofolate Reductase†

Stephanie N. Hicks, R. Derike Smiley, J. Bradley Hamilton,‡ and Elizabeth E. Howell*

Department of Biochemistry and Cellular and Molecular Biology, University of Tennessee, Knoxville, Tennessee 37996-0840

Received April 23, 2003; Revised Manuscript Received July 3, 2003

ABSTRACT: R67 dihydrofolate reductase (DHFR), which catalyzes the NADPH dependent reduction of dihydrofolate to tetrahydrofolate, belongs to a type II family of R-plasmid encoded DHFRs that confer resistance to the antibacterial drug trimethoprim. Crystal structure data reveals this enzyme is a homotetramer that possesses a single active site pore. Only two charged residues in each monomer are located near the pore, K32 and K33. Site-directed mutants were constructed to probe the role of these residues in ligand binding and/or catalysis. As a result of the 222 symmetry of this enzyme, mutagenesis of one residue results in modification at four related sites. All mutants at K32 affected the quaternary structure, producing an inactive dimer. The K33M mutant shows only a 2−4-fold effect on K_m values. Salt effects on ligand binding and catalysis for K33M and wildtype R67 DHFRs were investigated to determine if these lysines are involved in forming ionic interactions with the negatively charged substrates, dihydrofolate (overall charge of −2) and NADPH (overall charge of −3). Binding studies indicate that two ionic interactions occur between NADPH and R67 DHFR. In contrast, the binding of folate, a poor substrate, to R67 DHFR·NADPH appears weak as a titration in enthalpy is lost at low ionic strength. Steady-state kinetic studies for both wild type (wt) and K33M R67 DHFRs also support a strong electrostatic interaction between NADPH and the enzyme. Interestingly, quantitation of the observed salt effects by measuring the slopes of the log of ionic strength versus the log of k_{cat}/K_m plots indicates that only one ionic interaction is involved in forming the transition state. These data support a model where two ionic interactions are formed between NADPH and symmetry related K32 residues in the ground state. To reach the transition state, an ionic interaction between K32 and the pyrophosphate bridge is broken. This unusual scenario likely arises from the constraints imposed by the 222 symmetry of the enzyme.

Dihydrofolate reductases (DHFRs)[1] are ubiquitous enzymes that catalyze the NADPH dependent reduction of 5,6-dihydrofolate (DHF) to form 5,6,7,8-tetrahydrofolate (THF). The formation of THF is important since it is a precursor for purine nucleosides, methionine, and many other metabolites (*1*). Thus, inhibition of this enzyme results in disruption of DNA synthesis and consequently cell death. Trimethoprim (TMP) is a clinically important inhibitor of bacterial DHFRs. However, R67 DHFR, a type II R-plasmid encoded DHFR, confers resistance to TMP upon its hosts. This enzyme has no sequence or structural homology to other known DHFRs. Therefore, to gain more insight into the catalytic mechanism of this enzyme, the role of ionic interactions in ligand binding and catalysis was investigated.

† This work was supported by NSF Grant MCB-0131394 (E.E.H.).

* Corresponding author. Phone: (865) 974-4507. Fax: (865) 974-6306. E-mail: lzh@utk.edu.

‡ Present address: Upstate Inc., 706 Forest St., Charlottesville, VA 22903.

[1] Abbreviations: R67 DHFR, R67 dihydrofolate reductase; DHF, dihydrofolate; ITC, isothermal titration calorimetry; NADPH, nicotinamide adenine dinucleotide phosphate (reduced); PABA-glu, para-aminobenzoic acid tail of folate; TMP, trimethoprim; wt, wild-type; MTA buffer, 100 mM Tris, 50 mM Mes, 50 mM acetic acid polybuffer; μ, ionic strength; TE buffer, 10 mM Tris, 1 mM EDTA. Mutant enzymes possessing amino acid substitutions are named by the wild-type residue and the numbered position in the sequence. This enzyme is a homotetramer when a single residue is mentioned; all four related residues are implied.

The crystal structure of R67 DHFR was previously solved by Narayana et al. (*2*). Each monomer is a five stranded β-barrel consisting of 78 amino acids that self-associate to form the active tetramer. R67 DHFR contains a single active site pore formed from each of the four identical subunits (Figure 1). This pore possesses 222 symmetry and contains four possible binding sites. Because of steric constraints, the pore can only accommodate two ligands simultaneously. Two folate molecules were observed by time-resolved fluorescence anisotropy and isothermal titration calorimetry (ITC) data to bind in the pore. ITC also revealed that only two NADPH molecules bind in the pore (*3*). The active ternary complex consists of one molecule of NADPH and one molecule of DHF. Preferential formation of the active complex occurs due to negative cooperativity in binding between NADPH molecules and positive cooperativity between DHF and NADPH molecules (*3*).

Because of the symmetry of R67 DHFR, the active site pore is lined with a limited number of residues that can participate in catalysis including lysine 32, tyrosine 46, threonine 51, serine 65, valine 66, glutamine 67, isoleucine 68, and tyrosine 69 (*2*). Lysine 32 (K32) in each monomer is located near the dimer−dimer interface. The side chain NZ atom of K32 participates in hydrogen bonds with the backbone carbonyl groups of serine 34 and alanine 36 in a symmetry related monomer (*2*). The orientation of the K32 residue in each monomer is such that the side chain projects

10.1021/bi034643d CCC: $25.00 © 2003 American Chemical Society
Published on Web 08/22/2003

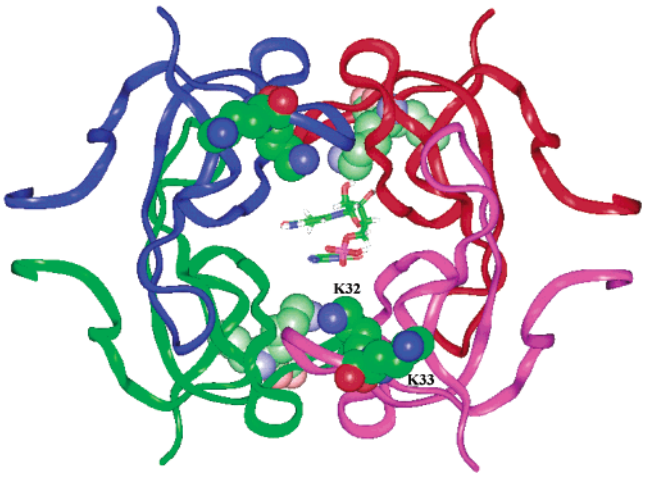

FIGURE 1: The active homotetrameric form of R67 DHFR is formed by the self-association of four identical subunits, A (blue), B (green), C (magenta), and D (red). K32 and K33 residues are shown in CPK format, and one set of the symmetry related residues are labeled at the lower right. The side chain of K32 projects into the active site pore, while K33 is located on the surface of the protein with its side chain projecting away from the active site pore. Two K32 and two K33 residues occur on one end of the pore pointing toward the viewer (lower right and upper left), while two symmetry related pairs occur on the other end of the pore, pointing away. The position of the ligands in the central pore is shown in stick format. The pteridine ring of folate (bottom) comes from the crystal structure (*2*) while that of the NMN moiety of NADPH (top) derives from docking studies (*4*). Carbon atoms are shown in green, oxygen atoms in red, nitrogen atoms in blue, and phosphate in magenta.

into the active site pore and has the potential to participate in ligand binding and catalysis (Figure 1). One proposed role of K32 is an ionic interaction with the 2′-phosphate off the AMP ribose ring of NADPH (ref *4* and N. Narayana, personal communication). To understand the role of the K32 residues in ligand binding, this residue was mutated to alanine, arginine, glutamine, and methionine. These mutations were made to either eliminate the possibility of an ionic contact with the substrates and/or to vary the potential for hydrogen bonding.

Lysine 33 (K33) is located on the surface of the enzyme with its side chain projecting away from the protein (Figure 1) (*2*). K33 was also mutated to the nonpolar uncharged residue, methionine. Since K32 and K33 are the only charged residues near the active site pore of wt R67 DHFR, mutagenesis of these residues to methionine allows investigation of their importance in forming ionic interactions with the substrates NADPH and DHF. If these residues are involved in an ionic contact(s) with the negatively charged substrates, then their replacement should result in weaker binding.

The importance of K32 and K33 in binding and catalysis is also illustrated by their conservation in type II DHFRs (*5*). Additionally, both K32 and K33 are proposed by Delphi, a finite-poisson difference solver, to be involved in generating a positive electrostatic potential at the active site that attracts the negatively charged substrates (NADPH and DHF) and facilitates binding (*4*).

MATERIALS AND METHODS

Mutagenesis. A synthetic R67 DHFR gene, cloned into a pUC8 vector (*6*), was used for PCR mutagenesis reactions. The oligonucleotide primers for the coding strand used to generate mutations in the R67 DHFR gene corresponding to the amino acid positions 32 and 33 using the Stratagene QuikChange Mutagenesis Kit were as follows: 5′GGGTGACCGCGTACGT**AAA**AAATCCGGAGCCGCC3′ (K32A), 5′GGGTGACCGCGTACGT**AGG**AAATCCGGAGCCGCC3′ (K32R), 5′GGGTGACCGCGTACGT**CAG**AAATCCGGAGCCGCC3′ (K32Q), 5′GGGTGACCGCGTACGT**ATG**AAATCCGGAGCCGCC3′ (K32M), and 5′GGGTGACCGCGTACGTAAG**ATG**TCCGGAGCCGCC3′ (K33M).

Mutants were verified by automated fluorescence DNA sequencing at the University of Tennessee DNA Sequencing Facility using an ABIPRISM Dye Terminator Cycle Sequencing Kit from Perkin-Elmer. Subsequently, R67 DHFR mutants were transformed into the SK383 strain of *Escherichia coli* for protein expression (*6*, *7*).

Protein Purification. Mutant R67 DHFR genes were expressed, and the protein was purified from *E. coli* grown to late stationary phase in TB media (*8*) at 37 °C in the presence of 200 μg/mL ampicillin and 20 μg/mL trimethoprim (TMP). K32M mutants were sensitive to the presence of TMP and therefore were first grown to visible turbidity before TMP addition. Purification was achieved by a series of steps including G-75 Sephadex, DEAE-Fractogel, and Hi-Q column chromatography. The final step of the purification procedure consisted of FPLC column chromatography using a Mono-Q anion exchange column. Purified protein was dialyzed into deionized water and lyophilized for storage at −20 °C.

Molecular Sieving Studies. To determine the apparent molecular weights of the K32A, K32M, and K33M mutant proteins, gel filtration using a Superose 12 (HR 10−30) column on a Pharmacia FPLC was performed at 4 °C. These studies were conducted at both pH 8 and pH 5 in MTA buffer (50 mM Mes, 100 mM Tris, 50 mM acetic acid). This buffer maintains a constant ionic strength ($\mu = 0.15$) from pH 4−10 (*9*). The K_{av} = (elution volume − void volume)/(bed volume − void volume) was calculated for protein standards from the Pharmacia Gel Filtration Calibration Kit to generate a standard curve from which the molecular weight of the R67 DHFR variants was determined.

pH Dependence of Oligomeric State. Tryptophan residues were used to monitor the intrinsic fluorescence of the lysine mutants as compared to wild-type protein to determine the pH dependent tetramer to dimer equilibrium. The model for the pH dependent equilibrium of R67 DHFR is

$$T + 2nH^+ \overset{K_{overall}}{\rightleftharpoons} 2DH_n \qquad (1)$$

where T is tetramer, D is dimer, DH_n is protonated dimer, and $K_{overall}$ equals K_a^{2n}/K_d. This model is based on the findings of Nichols et al. (*10*), where dissociation of the tetramer into dimers is linked to the protonation of symmetry related H62 residues located at the dimer−dimer interfaces.

Fluorescence measurements were made using a Perkin-Elmer LS-5B spectrometer interfaced to an IBM PS/2 computer. Tryptophan residues were excited at 295 nm, and emission was monitored from 300 to 450 nm using 2 μM wt, K32M, or K33M R67 DHFRs in MTA polybuffer. Each sample was titrated with small aliquots of 1 N HCl, and the pH was measured over the range of pH 8−4. The intensity

averaged emission wavelength, $\langle\lambda\rangle$, for each emission spectrum was calculated using

$$\langle\lambda\rangle = \sum(I_i \lambda_i)/\sum(I_i) \quad (2)$$

where I is intensity, and λ is the wavelength (*11*). The fluorescence data were fit to eq 5 in Nichols et al. (*10*) using a nonlinear regression subroutine of the Statistical Analysis Systems package (SAS, Cary, NC). Finally, fitting to the following equation normalized the data:

$$F_{app} = (Y_{obs} - Y_{pH8})/(Y_{pH4} - Y_{pH8}) \quad (3)$$

where F_{app} is a fractional value between 0 and 1, and Y_{obs}, Y_{pH8}, and Y_{pH4} are the optical values associated with the observed pH and with the pH limits of 8 and 4, respectively.

This same analysis was performed with 2 μM wild-type R67 DHFR in MTA buffer pH 8 ($\mu = 0.15$). NaCl was added to adjust the ionic strength to 0.25, 0.5, and 0.75 to determine salt effects on the pH dependent oligomerization of wild-type R67 DHFR.

Fluorescence Quenching. Binding of NADPH to 2.5 μM R67 DHFR was monitored in TE buffer (10 mM Tris, 1 mM EDTA, pH 7) using tryptophan fluorescence as per Zhuang et al. (*12*). Data were fit to

$$Fl = F_o - 0.5F_o[P_{tot} + K_d + L_{tot} - [(P_{tot} + K_d + L_{tot})^2 - 4P_{tot}L_{tot})^{1/2}] \quad (4)$$

where Fl is the observed fluorescence, L_{tot} is the total ligand concentration, and P_{tot}, K_d, and F_o are variables describing the number of enzyme binding sites, dissociation constant, and fluorescence yield per unit concentration of enzyme, respectively (*13*).

Isothermal Titration Calorimetry. ITC experiments with NADPH or folate as titrant were performed in TE buffer pH 7 at 28 °C in the presence of NaCl to adjust the ionic strength. Protein concentrations used for these experiments varied between 100 and 150 μM. Binding affinities and enthalpies associated with binding were measured as previously described (*3*). Binding of NADPH or folate to wt R67 DHFR was measured using a Microcal VP isothermal titration calorimeter. The data were collected by an IBM personal computer running DSCITC Software and were fit using Origin version 5.0 software. Baseline correction of the data was performed by injecting ligand into buffer. ITC was also done with the K33M mutant to determine the ΔH and the associated K_d values for NADPH binding in MTA buffer pH 8. Finally, binding of folate to a 1:1 mix of R67 DHFR/NADPH was performed at 13 °C (in TE buffer, pH 7) as previously reported (*3*). Instrument design and operation are explained by Wiseman et al. (*14*).

Kinetic Analysis. Steady-state kinetic data for the K33M mutant were obtained using the computer program UVS (Softways) on a Perkin-Elmer λ3a spectrophotometer interfaced with an IBM PS/2 (*15*). Kinetic assays were performed at 30 °C in MTA polybuffer pH 7. The kinetic parameters $K_{m(DHF)}$, $K_{m(NADPH)}$, and k_{cat} were determined under subsaturating conditions by maintaining a constant concentration of one ligand while varying the concentration of the other ligand. This was done at five or more different subsaturating ligand concentrations. Data were globally fit using a nonlinear regression analysis performed by SAS (*16*). The extinction coefficients used were 28 000 M^{-1} cm^{-1} at 282 nm for DHF (*17*), 6220 M^{-1} cm^{-1} at 340 nm for NADPH (*18*), and 12 300 M^{-1} cm^{-1} at 340 nm for the reaction (*19*).

Kinetic analysis was also performed to determine ionic strength effects on the steady-state kinetic parameters for wt and K33M R67 DHFRs. These assays were conducted at 30 °C in TE buffer, pH 7 ($\mu = 0.02$) with NaCl added to adjust the ionic strength to 0.15, 0.22, 0.32, and 0.42. Salt effects were also examined using NaF (μ from 0.1 to 0.62) and NaSCN (μ from 0.1 to 0.18). Salt effects were also tested with wt R67 DHFR using the alternate cofactor, NADH. Kinetic assays were monitored at 360 nm to allow the use of higher ligand concentrations to bracket the K_m values. Extinction coefficients at this wavelength were calculated as 2630 M^{-1} cm^{-1} for DHF, 4020 M^{-1} cm^{-1} for NADH, and 5020 M^{-1} cm^{-1} for the reaction.

RESULTS

Effects of Mutations: Molecular Sieving Studies. The K32A, K32M, K32Q, and K32R mutants provided minimal resistance to TMP, while the K33M mutant readily allowed cell growth in media containing TMP. TMP sensitivity has previously been observed in mutants that destabilize the active homotetramer (*10*, *20*). Therefore, the oligomeric state of each purified mutant protein was analyzed by the elution pattern on a molecular sieving column at pH 8 and 5. At pH 8, wt R67 DHFR elutes as a tetramer; however, at pH 5, wt R67 DHFR elutes as a dimer (*10*). The K32M and K32A mutants have approximate molecular weights at both pH 8 and 5 that correspond to the dimeric form of R67 DHFR (data not shown). Since K32 occurs near the dimer−dimer interface, these four symmetry related mutations have a cumulative effect and destabilize the tetramer. In contrast, the K33M mutant has similar estimated molecular weights at pH 8 and 5 to wt R67 DHFR, suggesting that it maintains the homotetrameric form over the pH ranges of our experiments.

pH Dependence of Oligomeric State. To provide a more quantitative evaluation of the effect of the mutations on the tetramer to dimer equilibrium, tryptophan fluorescence was monitored as a function of pH. Specifically, the tryptophan 38 (W38) residues that occur at the dimer−dimer interface can be utilized to monitor changes in the local environment since in the tetrameric form of R67 DHFR these residues are buried in a hydrophobic environment, whereas in the dimeric form of R67 DHFR these residues are solvent exposed. This equilibrium is linked to the protonation of histidine residues. Titration of the four symmetry related histidine 62 residues located at the dimer−dimer interfaces results in protonation and destabilization of the tetramer into dimers (*10*).

pH titrations for wt, K32M, and K33M R67 DHFRs are shown in Figure 2A. The wt and K33M enzymes show a titration consistent with a tetramer (pH 8) to two dimers (pH 5) transition. In contrast, the K32M (and K32A not shown) mutant does not, consistent with it remaining dimeric throughout this pH range. The pH titration data for wt and K33M R67 DHFRs were fit (*10*), and best-fit values are given in Table 1. The $K_{overall}$ value for the K33M mutant is similar to that for wt R67 DHFR, where the best fit occurs with $2n = 3$, and $2n$ represents the number of protons added

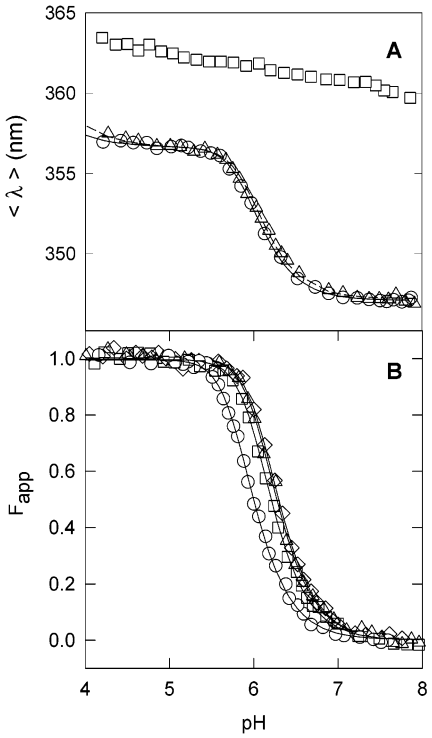

FIGURE 2: pH titrations to monitor the oligomeric state of R67 DHFR. Panel A, use of pH to monitor the effect of mutations on tetramer stability. $\langle\lambda\rangle$ is the intensity averaged emission wavelength. At pH 8, wt R67 DHFR is a tetramer, while at pH 5 it is a dimer. Data for wt R67 DHFR are represented by ○ points, K32M by □, and K33M by △. Best fits are represented by a solid line for wt R67 DHFR and a dashed line for K33M R67 DHFR (*10*). $K_{overall}$ values are given in Table 1 for $2n = 3$. Since the K32M data do not show a transition and the center of mass value corresponds more closely to the wt dimer value, we conclude that the K32M mutant remains dimeric throughout this pH range. Panel B, effects of increasing salt on the pH dependent oligomeric state of wt R67 DHFR were monitored at NaCl concentrations of 0 M (○), 0.25 M (□), 0.5 M (◇), and 0.75 M (△). Addition of salt shifts the titration; however, the effect is not great. Best-fit values are given in Table 1.

Table 1: Best-Fit Values for the $T + 2nH^+ \rightleftharpoons 2DH_n$ Equilibrium Monitored by Fluorescence

DHFR species/condition	$K_{overall}$ ($=K_a^{2n}/K_d$) for $2n = 3$ in units of M^2
wt R67 DHFR	$2.5 \times 10^{-13} \pm 9.1 \times 10^{-15}$
K33M R67 DHFR	$1.1 \times 10^{-13} \pm 6.1 \times 10^{-15}$
wt R67 DHFR (0.25 M NaCl)	$5.9 \times 10^{-14} \pm 2.9 \times 10^{-15}$
wt R67 DHFR (0.5 M NaCl)	$3.8 \times 10^{-14} \pm 2.0 \times 10^{-15}$
wt R67 DHFR (0.75 M NaCl)	$3.3 \times 10^{-14} \pm 1.5 \times 10^{-15}$

to the dimer−dimer interfaces resulting in dissociation of the tetramer. Since the K33 residues are located on the surface of the protein at the edge of the active site pore, the mutation was expected to have a minimal effect on the oligomeric state of the enzyme. Accordingly, the $K_{overall}$ values are similar to wt R67 DHFR.

Tryptophan fluorescence as a function of pH was also monitored with wt R67 DHFR in the presence of 0.25, 0.5, and 0.75 M NaCl to determine the effects of salt on the oligomeric state of the protein (Figure 2B). Addition of salt slightly destabilizes the tetramer. At pH 7, where most of the kinetic and binding experiments were performed, the majority of the protein is tetrameric so any observed salt effects are not due to a shift in the tetramer to dimer equilibrium.

Table 2: Comparison of Steady-State Kinetic Values for K33M and wt R67 DHFRs in MTA Buffer, pH 7

DHFR species	$K_{m(NADPH)}$ (μM)	$K_{m(DHF)}$ (μM)	k_{cat} (s^{-1})
wt R67 DHFR[a]	3.0 ± 0.06	5.8 ± 0.02	1.3 ± 0.07
K33M R67 DHFR	12 ± 1.8	14 ± 0.09	1.7 ± 0.13

[a] From Reece et al. (*6*).

Table 3: Binding of NADPH to wt and K33M R67 DHFRs in MTA Buffer (pH 8) as Measured by ITC

DHFR species	$K_{d1(NADPH)}$ (μM)	ΔH_1 (cal/mol)	$K_{d2(NADPH)}$ (μM)	ΔH_2 (cal/mol)
wt R67 DHFR[a]	2.5 ± 0.15	-8600 ± 200	95 ± 4.0	-5800 ± 250
K33M DHFR	19 ± 0.3	-6500 ± 22	630 ± 29	-530 ± 55

[a] Data from Bradrick et al. (*3*).

Binding and Steady-State Kinetic Analysis. Steady-state kinetics were performed with wt and mutant DHFRs (Table 2). Kinetic analysis of the K32M mutant could not be readily performed due to its low activity. The low activity correlates with a loss of the active site pore upon dimer formation. Previous kinetic analysis of dimeric R67 DHFRs indicates low activity (*10*, *20*); however, the activity of the K32 mutants is even lower, suggesting an additional affect of the mutation on binding and catalysis. In contrast, steady-state kinetics could be performed for the K33M mutant. This mutant displays a 2-fold increase in the K_m for DHF and a 4-fold increase in the K_m for NADPH. There was also a slight increase in k_{cat}. Additionally, binding of NADPH to this mutant was monitored by ITC (Table 3). Negative cooperativity is observed during NADPH binding, with one tight site and one weak site. The K33M mutation weakens binding to these sites by 8- and 7-fold, respectively. Together, these results suggest that K33, located on the surface of R67 DHFR, plays a minor role in binding both cofactor and substrate in the active site pore.

Ionic Strength Effects. Since the role of K32 could not be evaluated directly through a site-directed mutagenesis approach, its ability to participate in ionic interactions was evaluated through salt effects on wt and K33M R67 DHFRs. Ligand binding was first evaluated, followed by steady-state kinetic analysis.

Fluorescence Quenching with NADPH. The binding of NADPH as affected by ionic strength was determined by monitoring fluorescence quenching. The sensitivity of this technique only allows monitoring of binding at the first tight site, K_{d1}. As the ionic strength is increased ($\mu = 0.04-0.27$), the $K_{d1(NADPH)}$ also increases (0.35−20 μM). The slope of a log−log plot of $K_{d1(NADPH)}$ versus ionic strength is 2.0 ± 0.3 (Figure 3). The slopes of these types of plots have previously been taken to describe *Z*, the number of ionic interactions involved in binding (*21*−*23*). Because of the high K_{d1} associated with the binding of DHF (125 μM), $K_{d(DHF)}$ values could not be measured using this approach.

ITC with NADPH. To gain additional information on the effects of ionic strength on NADPH binding, ITC was also used. The shape of the titration curves varied, with a sigmoidal plot observed at $\mu = 0.02$ and a hyperbolic plot at $\mu = 0.32$. At high ionic strength, the second molecule of NADPH either does not bind (i.e., cooperativity is altered) or binding becomes sufficiently weak so that we are unable

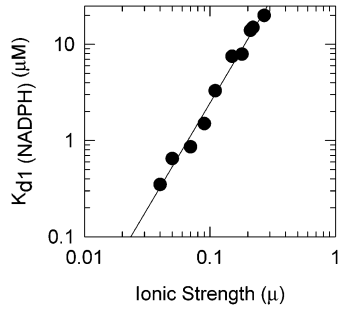

FIGURE 3: Log−log plot of $K_{d1\ (NADPH)}$ vs ionic strength. The K_d was determined by the quenching of R67 DHFR fluorescence upon NADPH addition. Errors on the values are smaller than the symbol size and typically are <10%. As the ionic strength is increased, $K_{d1\ (NADPH)}$ increases.

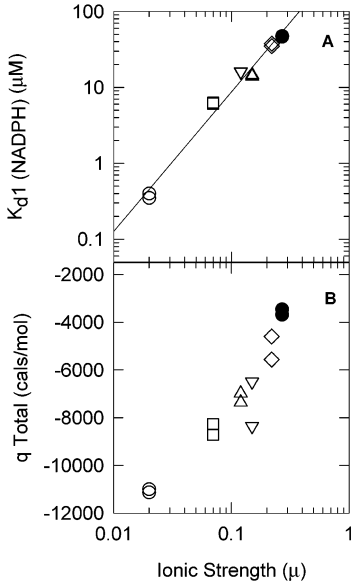

FIGURE 4: Effects of increasing ionic strength on binding of NADPH to wt R67 DHFR as monitored by ITC. As ionic strength increases, binding weakens as shown in panel A. K_{d1} values were able to be measured at all ionic strengths, and errors are smaller than the symbol size (typically <10%). The corresponding q_{Total} values decrease as the ionic strength increases as shown in panel B. Experiments were performed at ionic strengths of 0.02 (○), 0.07 (□), 0.12 (△), 0.15 (▽), 0.22 (◇), and 0.32 (●).

to saturate this site. This suggested the use of a single site model for fitting, and at intermediate values of μ, fitting to this model gave reasonable fits. (Also, fitting to two sites consistently yielded one K_d equivalent to the single site model.) Values obtained from these titrations are shown in Figure 4. $K_{d1(NADPH)}$ increases from 0.4 to 47 μM as μ increases from 0.02 to 0.3. The slope of the log−log plots for $K_{d1(NADPH)}$ versus ionic strength is 1.8 ± 0.08. In addition, the total heat evolved (q_{Total}) decreases with increasing ionic strength, consistent with the loss of ionic interactions. These results, in conjunction with the fluorescence quenching data above, indicate that two ionic interactions are involved in binding the first NADPH molecule.

Isothermal Titration Calorimetry with Folate. ITC was also used to monitor salt effects on folate binding. The poor substrate, folate, was used in these experiments instead of DHF, as salt destabilizes DHF over the time period required to run an ITC experiment. Folate is similar in structure to DHF except that it possesses a double bond between C7 and N8. In these experiments, we are unable to consistently fit

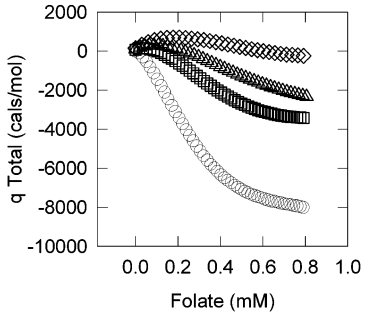

FIGURE 5: Effects of ionic strength on the total heat of folate binding as measured by ITC. The protein concentration was 100 μM for all experiments. The total heat observed upon folate addition is plotted at various ionic strengths (μ = 0.15 (○), μ = 0.22 (□), μ = 0.27 (△), and μ = 0.32 (◇)).

Table 4: ITC Data for Folate Binding to a 1:1 Mixture of R67 DHFR•NADPH at 13 °C in TE Buffer (pH 7) in the Presence of Various Salt Concentrations to Adjust the Ionic Strength[a]

ionic strength	K_d (μM)	n	ΔH (cal/mol)	no. of experiments
0.02	11.0 ± 0.4	0.95	−13100 ± 180	2
0.07	20.0 ± 1.0	1.0	−13300 ± 390	2
0.15	15.2 ± 0.4	1.0	−8300 ± 67	2
0.22	9.5 ± 0.7	0.98	−5700 ± 130	2
0.27	13.3 ± 0.8	0.99	−5800 ± 150	2
0.32	12.8 ± 0.8	1.1	−5700 ± 100	2

[a] The data were fit to a single site model using the Origin software.

the titrations for folate binding to two sites, suggesting the occurrence of an additional process during binding. One possibility might involve some effect associated with binding of folate dimers from solution. Dimerization of folate has previously been reported (*24*). Even with this potential complication, we can qualitatively note the effect of increasing ionic strength on folate binding by plots of total enthalpy (q_{Total}) versus folate concentration. This plot reveals that the binding process is less exothermic (i.e., involves lower enthalpy values) as the concentration of salt increases (Figure 5). Increasing μ has a clear effect; however, we are unable to extract the number of interactions disrupted.

Binding of folate to a 1:1 mixture of R67 DHFR•NADPH was also performed in varying salt concentrations. One folate molecule binds to form the ternary complex, and the K_d values in Table 4 show no evidence of a titration. However, a titration is observed when the ΔH values are evaluated. At low ionic strength, ΔH remains constant at approximately −13 000 cal/mol. Only one intermediate point was monitored before a second plateau in ΔH is observed (at approximately −5800 cal/mol). This titration indicates that folate binding is salt dependent in the ternary complex, and since the titration is complete by a μ of 0.22, the ionic interaction must be weaker than those observed in either the two NADPH or the two folate complexes.

Steady-State Kinetic Analysis in the Presence of Salt. Salt effects on steady-state kinetics were also performed with wt and K33M R67 DHFRs to investigate further the importance of ionic interactions in ligand binding and catalysis. As the buffer is changed from MTA to TE, minor differences in K_m are noticed. More interestingly, as the ionic strength is increased, the binding of both cofactor and substrate is weakened. In addition, the k_{cat} values increase. Concentrations of up to 0.4 M NaCl were used to examine salt effects.

Table 5: Slopes of the Log−Log Plots for $k_{cat}/K_{m(NADPH)}$, $k_{cat}/K_{m(DHF)}$, k_{cat}, and K_ms as a Function of Ionic Strength for wt and K33M R67 DHFRs in the Presence of NaCl, NaF, or NaSCN

R67 DHFR species (salt)	slope of $k_{cat}/K_{m(NADPH)}$ plot	slope of $k_{cat}/K_{m(DHF)}$ plot	slope of k_{cat} plot	slope of $K_{m(NADPH)}$ plot	slope of $K_{m(DHF)}$ plot
wt R67 DHFR (NaCl)	-0.6 ± 0.09	-0.9 ± 0.03	0.9 ± 0.08	1.5 ± 0.1	1.8 ± 0.2
wt R67 DHFR (NaF)	-0.9 ± 0.2	-0.8 ± 0.08	0.9 ± 0.2	1.7 ± 0.4	1.6 ± 0.2
wt R67 DHFR (NaSCN)	-1.6 ± 0.2	-1.5 ± 0.2	0.7 ± 0.3	2.2 ± 0.2	2.2 ± 0.2
K33M DHFR (NaCl)	-0.7 ± 0.03	-0.9 ± 0.09	1.0 ± 0.3	1.7 ± 0.2	1.9 ± 0.4

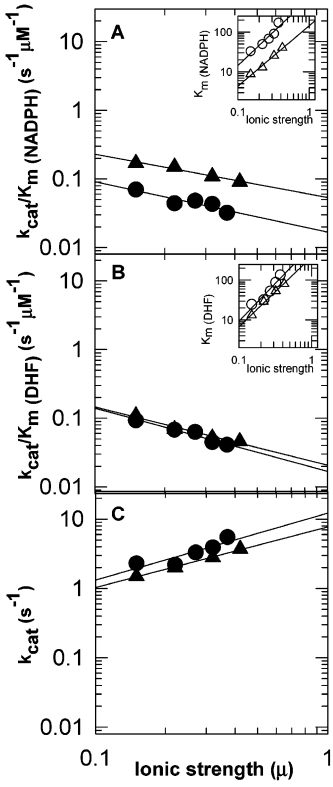

FIGURE 6: Log−log plots of steady-state kinetic values vs ionic strength. Steady-state kinetics were performed with wt (▲, △) and K33M (●, ○) R67 DHFRs in the presence of increasing NaCl concentrations. Panels A and B show the effects on k_{cat}/K_m with insets showing the effects on the respective K_ms. Panel C shows the effect of increasing salt on k_{cat}. The slopes associated with the plots are given in Table 5.

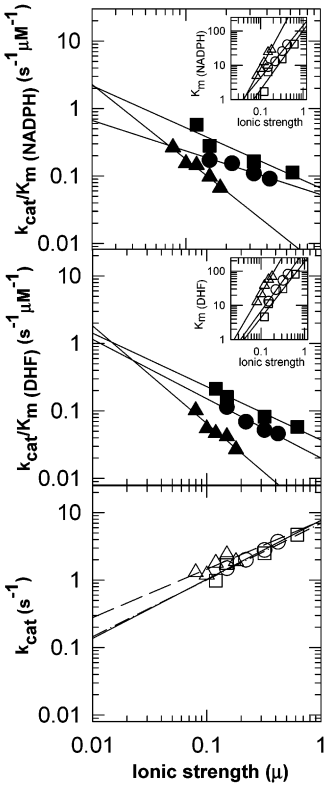

FIGURE 7: Steady-state kinetics were performed with wt R67 DHFR in NaF (■, □) and NaSCN (▲, △) and compared to the kinetic values obtained in the presence of NaCl (●, ○). The plots of log k_{cat}/K_m vs log ionic strength reveal a different slope in the presence of SCN^-. The slopes for these plots are listed in Table 5.

To quantify the number of ionic interactions involved in ligand binding and catalysis, log−log plots of the steady-state kinetic data versus ionic strength were generated. These plots are shown in Figure 6, and their corresponding slopes are given in Table 5. Surprisingly, there is a linear relationship between ionic strength and k_{cat} for the R67 DHFR reaction. The slope of the log−log plot for the wt enzyme is 0.9 ± 0.08. Additionally, slopes of 1.8 ± 0.2 and 1.5 ± 0.1 for the log−log plots of ionic strength versus $K_{m(DHF)}$ and $K_{m(NADPH)}$ are observed for wt R67 DHFR. Finally, since the ionic strength effects on k_{cat} result in rate enhancements (slope effects of ~1), while salt effects on K_m are consistent with weaker binding (slope effects of ~2), the overall effect on k_{cat}/K_m is a net decrease in catalytic efficiency (slope effects of approximately −1). These results, in conjunction with the above binding studies, suggest a model where two salt sensitive interactions are involved in initial ligand binding; however, one of these interactions is lost as the ground state proceeds toward the transition state.

A comparison of the salt effects on wt and K33M R67 DHFRs shows that the slopes of the various plots are quite similar (Table 5). We conclude that K33 is not the residue responding to the presence of salt.

Effect of Different Salts on Binding. To evaluate if these salt effects on wt R67 DHFR are due to a nonspecific and/or a salt specific effect resulting in the disruption of an ionic interaction, kinetic characterization was also performed in the presence of NaF as well as NaSCN (*25*−*27*). The steady-state data are given graphically in Figure 7. The abbreviated Hofmeister series (SCN^-, I^-, Br^-, Cl^-, F^-) indicates that F^- has a high charge density and a high energy of hydration, making it least able to compete with a charged ligand for binding. Cl^-, in the middle of the Hofmeister series, has a neutral effect, while SCN^-, with a lower charge density and lower energy of hydration, is more able to compete for binding (*25*−*28*). Thus, the use of different salts allows specific anion effects to be discerned from ionic strength effects. While the absolute values for k_{cat} and K_m are somewhat different, a comparison of the slopes for the NaCl and NaF plots yields values within error of each other, suggesting that there is not a significant difference depending on the anion type (Table 5). However, extending

Table 6: Steady-State Kinetic Values for wt R67 DHFR with NADH in the Presence of 0.3 M NaCl TE, pH 7

wt R67 DHFR cofactor (ionic strength)	$K_{m(cofactor)}$ (μM)	$K_{m(DHF)}$ (μM)	k_{cat} (s^{-1})
NADH ($\mu = 0.32$)	320 ± 17	250 ± 16	0.7 ± 0.04
NADPH ($\mu = 0.32$)	26 ± 1.3	54 ± 2.5	2.8 ± 0.1

the comparison to NaSCN shows a different slope for k_{cat}/K_m values, suggesting the presence of specific anion effects.

NADPH versus NADH Binding. To probe whether the 2′-phosphate off the adenine ribose of NADPH is involved in one of the ionic interactions with wt R67 DHFR, the alternate cofactor NADH was used in steady-state kinetic analysis. DHF inhibition is noted, particularly at low ionic strengths, perhaps arising from weaker binding of NADH and less positive cooperativity between NADH and DHF, which allows more ready formation of the inhibitory 2DHF complex. Since fitting data sets displaying inhibition using SAS requires some knowledge of the various K_ds involved (*16*), we did not pursue them. A qualitative observation is that the rate clearly increases with increasing salt concentration, as do the K_m values. That the rate increases using either NADPH or NADH as cofactor while ionic strength concurrently increases suggests that the ionic interaction broken going from the ground to transition state involves the PP_i bridge since this is the common negatively charged moiety.

There is no obvious DHF inhibition observed when NADH is used at $\mu = 0.32$ and the steady-state kinetic data can be fit. Table 6 shows that the K_m for NADH is 12-fold higher than that for NADPH and that the k_{cat} value is decreased 4-fold. This combines to increase $k_{cat}/K_{m(cofactor)}$ 50-fold. The K_m for DHF is also affected, being 4.6-fold higher. Measurements of K_m values for NADH were not made beyond an ionic strength of 0.32 due to limitations in the range of the spectrophotometer. Hence, log−log plots to evaluate the number of ionic contacts with NADH as compared to NADPH were not generated. An increase in $K_{m(NADH)}$ as compared to $K_{m(NADPH)}$ for R67 DHFR has previously been observed by Smith and Burchall (*29*). Similar fold effects have also been seen in *E. coli* DHFR where R44L and H45Q mutations were constructed to evaluate the role of these residues in binding the 2′-phosphate and PP_i moieties of NADPH (*30*). The R44L and H45Q mutations altered the K_d for NADPH (monitored by fluorescence quenching) by 11- and 6-fold, respectively, while binding of dihydrofolate was unaltered. Effects on the hydride transfer step were 21- and 3-fold decreases, respectively. Together, these data illustrate the importance of the 2′-phosphate moiety in different DHFR scaffolds by the large effects on binding in the absence of this group.

DISCUSSION

The role of ionic interactions in binding and catalysis in R67 DHFR has been investigated. The following observations indicate that ionic interactions play a role in these processes. (1) Fluorescence quenching and ITC data reveal that $K_{d1(NADPH)}$ increases with increasing ionic strength. (2) ITC experiments show that the total heat associated with NADPH binding becomes less negative as ionic strength increases. (3) ITC data demonstrate binding of two folate molecules is a salt sensitive process. (4) Calorimetry experiments show a titration in ΔH for folate binding to R67 DHFR·NADPH that is complete by a μ of 0.22. (5) Salt effects are observed by monitoring the steady-state kinetic behavior of the wt enzyme in buffers of increasing ionic strength. Higher K_m values for NADPH and DHF are observed as the salt concentration increases as well as an enhancement of k_{cat}. (6) Similar salt induced slope effects are observed for the wt and K33M enzymes. The only charged residues near the active site in this mutant are the symmetry related K32 residues. (7) Our mutagenesis studies implicate only a minor role for K33 in binding illustrated by the 2−4-fold weaker K_m values for the K33M mutant. The fold changes associated with the K33M mutant are smaller than the observed salt effects. (8) There is a 50-fold effect on $k_{cat}/K_{m(cofactor)}$ in the presence of NADH at $\mu = 0.32$, suggesting that the 2′-phosphate is involved in an ionic interaction with R67 DHFR. (9) pH titration studies reveal that increasing the concentration of NaCl up to 0.75 M does not affect the stability of the enzyme.

Quantitation of the Number of Ionic Interactions Involved in Ligand Binding. Quantitating the number of ionic interactions involved in ligand binding was first described by Record et al., in 1976, using various proteins binding to DNA (*21*). Recently, Park and Raines (*22*) have described the requirements for quantitating the number of ionic interactions involved in ligand binding and catalysis using salt-rate profiles. One of the conditions is that an increase in the concentration of salt does not cause a decrease in the stability of the enzyme. pH titration studies with wt R67 DHFR reveal that increasing the NaCl concentration up to 0.75 M does not significantly affect the stability of this enzyme. In addition, to be able to use salt effects to quantitatively monitor ionic interactions, the k_{cat} should reflect the chemical step, not product release (*22*). Hydride transfer is the rate-determining step in the R67 DHFR reaction as monitored by NADPD isotope effects (*31*). Another preference is for the assays to be monitored at the pH optimum to minimize any pH effects. This criterion was not met with respect to R67 DHFR, as activity increases as the concentration of protonated DHF increases (N5 pK_a of 2.59) (*31*, *32*). This titration is masked, however, as the active site pore in the wt homotetramer is lost upon dissociation into dimers (Figure 2A). While this criterion was not met, the assay pH was carefully maintained at pH 7.0, and any systematic alterations in pH should be minimal and would not be expected to propagate into large (unitary) slope effects. Finally, a variance of the anion character should minimally affect the slope of the resulting plots. While the slopes describing steady-state kinetic parameters of R67 DHFR are similar in NaCl and NaF, higher slopes for k_{cat}/K_m are observed in NaSCN. A different effect by SCN^- suggests the additional presence of specific anion effects. A recent study of lysozyme crystal structures obtained in different salts (NaI, $NaNO_3$, KSCN, and *p*-toluene sulfonate) shows the presence of common anion sites as well as specific sites (*33*). Binding strategies include contacts with Arg and Lys side chains as well as H-bonds with other residues (either side or main chain). Thus, while specific anion sites do appear to occur in R67 DHFR, the likelihood of common anion sites remains reasonable. Another instance of general ionic strength effects augmented by specific anion effects has also been noted by Lee et al. in measuring different salt effects on the pK_as of histidines in *Staphylcoccal* nuclease (*34*).

How Many Ionic Interactions Are Involved in Ligand Binding? Log−log plots of $K_{d(NADPH)}$ versus ionic strength, from both fluorescence quenching and ITC studies, display slopes of ~2. These combined results suggest that two ionic interactions are likely to be involved in binding the first NADPH molecule in the presence of NaCl. This is also confirmed by a 50-fold decrease in catalytic efficiency using NADH as a cofactor (involvement of 2′-phosphate) as well as a salt effect on k_{cat} using NADH.

We have been unable to obtain K_d values for DHF/folate by either fluorescence quenching or ITC under various salt conditions. However, folate binding under binary complex conditions is salt sensitive as shown in Figure 5. In contrast, folate addition to the R67 DHFR·NADPH complex shows no change in K_d values coupled to a titration in enthalpy that is complete by a μ of 0.22. These results suggest different salt sensitivities for the R67 DHFR·2 folate and R67 DHFR·NADPH·folate complexes.

The observation that the K_d for folate binding to the ternary complex does not vary while a titration in ΔH is observed invokes enthalpy−entropy compensation (*35*−*38*). In this process, the unvarying K_d describes ΔG as $\Delta G = -RT \ln K_a$ where K_a is the association constant and equals $1/K_d$. For a titration in ΔH to occur, coupled with a constant ΔG value, suggests a compensating change in entropy (from the relationship $\Delta G = \Delta H - T\Delta S$). These results suggest a catalytic strategy to minimize effects on the productive ternary complex as compared to the nonproductive complexes. Specifically, binding of folate at low salt involves at least one ionic interaction, which is lost by $\mu = 0.22$. Loss of the ionic interaction could readily be compensated for by a decreased desolvation penalty. In other words, ions are strongly solvated, and to form an ion pair, both ions must be desolvated; this process opposes ion pair formation (*39*).

Why Does k_{cat} Increase with Increasing Ionic Strength? In the kinetic studies with wt and K33M R67 DHFRs, an increase in k_{cat} is observed with increasing ionic strength. This observation is unusual as Park and Raines (*22*) note that in most enzymes, the ground state resembles the transition state, and changes in ionic interactions typically do not occur. However, these observations are not totally unprecedented as increases in k_{cat} have been observed with the NADPH-cytochrome oxidoreductase-cytochrome *c* complex (*40*) as well as the herpes simplex virus protease in the presence of increasing ionic strength (*41*). The slope of the log−log plot of k_{cat} versus ionic strength (NaCl) in wt R67 DHFR is approximately one. The increased rate could potentially arise if salt increased the N5 pK_a of DHF since protonated DHF is the productive substrate for R67 DHFR (*31*). However Cocco et al. (*42*) find that this pK_a is not significantly altered by increased ionic strength. Therefore, an increase in the concentration of protonated DHF is probably not responsible for the increase in k_{cat}. A second possibility for the increase in k_{cat} might be due to a larger destabilization of the ground state relative to the transition state as μ increases. This would result in a decrease in the activation energy barrier to reach the transition state and an increased k_{cat}. This argument is supported by a slope of 2 for the log−log plots of $K_{d(NADPH)}$ versus ionic strength contrasted with a subsequent decrease in the slope to 0.6−0.7 for the log−log plots of $k_{cat}/K_{m(NADPH)}$ versus ionic strength. The data in Figure 6C indicate that transition state binding is different than ground state binding and that one salt bridge is broken as the ground state moves to the transition state.

Which Residues in R67 DHFR Are Involved in Ionic Interactions with the Ligands? There are several possible binding models that would allow two ionic interactions between R67 DHFR and NADPH. The first model involves one K32 residue and one K33 residue binding to different ionic centers in NADPH. However, from the crystal structure, K32 appears on the binding surface of the active site pore making it more likely to be involved in a direct interaction than K33 (*2*). In addition, our docking studies indicate that symmetry related K32 residues are involved in binding both NADPH and DHF, while no direct interactions are predicted for K33 (*4*). Further, the salt effect observed for the K33M mutant is similar to the salt effect observed in wt R67 DHFR. In the K33M mutant, symmetry related K32 residues are the only positively charged residues remaining near the active site pore that possess the potential to be involved in ionic interactions with the substrates. Thus, this model can be eliminated. A second model involves two K32 residues, each from a different monomer of R67 DHFR, contributing separate ionic interactions. K32 (monomer A) could interact with the 2′-phosphate, while K32 (monomer C) would interact with the pyrophosphate bridge (Figure 1). This model appears reasonable and is similar to a docked model of NADPH (ref *4* and unpublished results).

A model for folate/DHF binding is less clear. From examination of the crystal structure, the two carboxylate groups from the Glu tail of DHF cannot span across the end of the pore to interact with two K32 residues from different monomers in R67 DHFR. This limitation suggests that only one ionic interaction can occur per bound DHF/folate. We were unable to support this model by quantitating the number of interactions involved in the formation of the two folate complexes. Also, the ITC data for folate addition to R67 DHFR·NADPH did not quantitate the number of interactions, but this interaction must be relatively weak as the ΔH titration is complete by $\mu = 0.22$. Previous studies supporting mobility for the Glu tail include electron density for only the pteridine rings in the crystal structure describing bound folate (*2*), interligand NOE data for the Glu tail in the R67 DHFR·$NADP^+$·folate complex (*43*), and numerous positions for the PABA-Glu tail of folate in docking studies to generate a reasonable model of the ternary complex (*4*).

Which Regions of NADPH Are Involved in Forming Ionic Contacts with R67 DHFR? K32 is conserved in all R-plasmid encoded variants, suggesting that it has a functional and/or structural role (*5*). It has been proposed that K32 interacts with the 2′-phosphate of NADPH (ref *4* and N. Narayana, personal communication). Kinetic studies using NADH as an alternate cofactor reveal a much lower k_{cat}/K_m for NADH as compared to NADPH at an ionic strength of 0.32. Since these molecules are identical in structure except for the substitution of a negatively charged phosphate at the 2′ position with a hydrogen, the observed effects on the NADH versus NADPH values are consistent with the 2′-phosphate forming an ionic interaction with wt R67 DHFR. NMR studies (Pitcher et al., in press) are also consistent with an ionic interaction between K32 and the 2′-phosphate of NADPH. Yet, two ionic interactions are predicted from the log−log plots of $K_{d(NADPH)}$ and $K_{m(NADPH)}$ versus ionic

strength. Therefore, there must be an additional ionic interaction between the pyrophosphate bridge of NADPH and the enzyme. This is supported by our qualitative observation that the rate increases with increasing salt concentration when NADH is used as a cofactor. That a rate increase occurs using either NADPH or NADH as a cofactor suggests that the ionic interaction broken going from the ground state to the transition state involves the PP_i bridge.

While the above model is consistent when all the NaCl data are taken into account, the observation that the NaSCN slope effects on k_{cat}/K_m are different indicate some degree of anion specificity and suggest that the above arguments must remain qualitative. While an Ocam's razor approach supports a simple pattern of binding and catalysis that is consistent with the above model, we cannot rule out more unusual effects arising from specific ion interactions, as well as the effect of salts on desolvation penalties, the extent of accumulation or exclusion of the solute from the protein surface, the result of charges propagating through a hydrophobic interior, long-range electrostatic interactions, or the effect of salt on water properties (*33*, *34*, *44*−*46*).

What Is the Role of K33? K33 is also conserved in all R-plasmid encoded variants, which suggests that it has a functional role as well. However, its role in binding is not as clear. The similar slopes for salt effects on the wt and K33M mutant enzymes indicate no direct ionic interaction between this residue and the ligands. It may be involved in properly positioning K32. Alternatively, K33, along with K32, may enhance the positive electrostatic potential at the active site pore of R67 DHFR to aid in binding (*4*, *47*).

It is interesting to note that the contiguous R31 residue is also conserved, as is E75, the side chain of which is in van der Waals contact with R31. R29 and E60 are also nearby, conserved and in close contact. A recent report notes that clusters of positively charged residues are rare and may be important in protein structure and function (*48*). Perhaps this charge grouping facilitates NADPH and folate binding.

Summary and Conclusions. DelPhi, a finite Poisson−Boltzmann difference solver, predicts that K32 and K33 generate a positive electrostatic potential at the active site pore of R67 DHFR (*4*). Numerous enzymes have been proposed to utilize an electrostatic potential to guide ligands into the active site where specific interactions can then occur for binding of substrate (*49*−*51*). A model for the role of electrostatics in ligand binding and catalysis in R67 DHFR suggests that K32 and K33 guide the negatively charged ligands to the active site pore by establishing a positive electrostatic potential. Once the ligands are proximal to the active site, symmetry related K32 residues likely contribute direct ionic interactions with NADPH and likely DHF (at very low salt). After formation of the ground state complex, at least one ionic interaction breaks, leading to hydride transfer. This key event probably involves the loss of an ionic interaction between the enzyme and the pyrophosphate bridge of NADPH. This scenario could permit the ligands to move toward the hourglass center of the pore, facilitate stacking between the pteridine and the nicotinamide rings as well as exclude solvent, and ultimately lead to the correct distance and angle for hydride transfer. This unusual mechanism could arise from the need to balance catalysis with the constraints of the structure (e.g., the 222 symmetry of the active site pore). For example, if two ionic interactions occur between NADPH and symmetry related K32 residues, then while the loss of one interaction (by a mutation) could enhance k_{cat}, the concurrent loss of the second symmetry associated interaction would necessarily decrease catalytic efficiency (k_{cat}/K_m). Introduction of asymmetry into the active site pore should help sort out these various models of catalysis and perhaps lead to enhanced activity.

ACKNOWLEDGMENT

Special thanks to Nathan VerBerkmoes for confirming mutant proteins by mass spectrometry.

REFERENCES

1. Kraut, J., and Matthews, D. A. (1987) *Biol. Macromol. Assem. 3*, 1−71.
2. Narayana, N., Matthews, D. A., Howell, E. E., and Xuong, N. (1995) *Nat. Struct. Biol. 2*, 1018−1025.
3. Bradrick, T. D., Beechem, J. M., and Howell, E. E. (1996) *Biochemistry 35*, 11414−11424.
4. Howell, E. E., Shukla, U., Hicks, S. N., Smiley, D. R., Kuhn, L. A., and Zavodsky, M. I. (2001) *J. Comput. Aided Mol. Des. 15*, 1035−1052.
5. Flensburg, J., and Steen, R. (1986) *Nucleic Acid Res. 14*, 5933.
6. Reece, L. J., Nichols, R., Ogden, R. C., and Howell, E. E. (1991) *Biochemistry 30*, 10895−10904.
7. Zeig, J., Maples, V. F., and Kushner, S. R. (1978) *J. Bacteriol. 134*, 958−966.
8. Tartof, K. D., and Hobbs, C. A. (1987) *Gibco-BRL Focus 9*, 12.
9. Ellis, K. J., and Morrison, J. F. (1982) *Methods Enzymol. 87*, 405−426.
10. Nichols, R., Weaver, C. D., Eisenstein, E., Blakley, R. L., Appleman, J., Huang, T.-H., Huang, F.-Y., and Howell, E. E. (1993) *Biochemistry 32*, 1695−1706.
11. Royer, C. A., Mann, C. J., and Matthews, C. R. (1993) *Protein Sci. 2*, 1844−1852.
12. Zhuang, P., Yin, M., Holland, J. C., Peterson, C. B., and Howell, E. E. (1993) *J. Biol. Chem. 268*, 22672−22679.
13. Dunn, S. M., Lanigan, T. M., and Howell, E. E. (1990) *Biochemistry 29*, 8569−8576.
14. Wiseman, T., Williston, S., Brandts, J. F., and Lin, L.-N. (1989) *Anal. Biochem. 179*, 131−137.
15. Howell, E. E., Warren, M. S., Booth, C. L. J., Villafranca, J. E., and Kraut, J. (1987) *Biochemistry 26*, 8591−8598.
16. Smiley, R. D., Stinnett, L. G., Saxton, A. M., and Howell, E. E. (2002) *Biochemistry 41*, 15664−15675.
17. Blakley, R. L. (1960) *Nature 188*, 231−232.
18. Horecker, B. L., and Kornberg, A. (1948) *J. Biol. Chem. 175*, 385−390.
19. Baccanari, D., Phillips, A., Smith, S. L., Sinski, D., and Burchall, J. (1975) *Biochemistry 14*, 5267−5273.
20. West, F. W., Seo, H.-S., Bradrick, T. D., and Howell, E. E. (2000) *Biochemistry 39*, 3678−3689.
21. Record, M. T. J., Lohman, T. M., and De Haseth, P. (1976) *J. Mol. Biol. 107*, 145−158.
22. Park, C., and Raines, R. T. (2001) *J. Am. Chem. Soc. 123*, 11472−11479.
23. Jensen, D. E., and von Hippel, P. H. (1976) *J. Am. Chem. Soc. 251*, 7198−7214.
24. Poe, M. (1973) *J. Biol. Chem. 246*, 7025−7032.
25. Grucza, R. A., Bradshaw, J. M., Mitaxov, V., and Waksman, G. (2000) *Biochemistry 39*, 10072−10081.
26. Fisher, B. M., Ha, J.-H., and Raines, R. T. (1998) *Biochemistry 37*, 12121−12132.
27. Relan, N. K., Jenuwine, E. S., Gumbs, O. H., and Shaner, S. L. (1997) *Biochemistry 36*, 1077−1084.
28. Collins, K. D. (1997) *Biophys. J. 72*, 65−76.
29. Smith, S. L., and Burchall, J. J. (1983) *Proc. Natl. Acad. Sci. 80*, 4619−4623.
30. Adams, J., Johnson, K., Matthews, R., and Benkovic, S. J. (1989) *Biochemistry 28*, 6611−6618.
31. Park, H., Zhuang, P., Nichols, R., and Howell, E. E. (1997) *J. Biol. Chem. 272*, 2252−2258.

32. Maharaj, G. S., Selinsky, B. S., Appleman, J. R., Perlman, M., London, R. E., and Blakley, R. L. (1990) *Biochemistry 29*, 4554−4560.
33. Vaney, M. C., Broutin, I., Retailleau, P., Douangamath, A., Lafont, S., Hamiaux, C., Prange, T., Ducruix, A., and Ries-Kautt, M. (2001) *Acta Crystallogr. D57*, 929−940.
34. Lee, K. K., Fitch, C. A., Lecomte, J. T. J., and Garcia-Moreno, E. B. (2002) *Biochemistry 41*, 5656−5667.
35. Gilli, P., Ferretti, V., Gilli, G., and Borea, P. A. (1994) *J. Phys. Chem. 98*, 1515−1518.
36. Dunitz, J. D. (1995) *Chem. Biol. 2*, 709−712.
37. Chervenak, M. C., and Toone, E. J. (1994) *J. Am. Chem. Soc. 116*, 10533−10539.
38. Grunwald, E., and Steel, C. (1995) *J. Am. Chem. Soc. 117*, 5687−5692.
39. Chong, L. T., Dempster, S. E., Hendsch, L. P., and Tidor, B. (1998) *Protein Sci. 7*, 206−210.
40. Shen, A. L., and Kasper, C. B. (1995) *J. Biol. Chem. 270*, 27475−27480.
41. Hall, D. L., and Darke, P. L. (1995) *J. Biol. Chem. 270*, 22697−22700.
42. Cocco, L., Blakley, R. L., Walker, T. E., London, R. E., and Matwiyoff, N. A. (1978) *Biochemistry 17*, 4285−4290.
43. Li, D., Levy, L. A., Gabel, S. A., Lebetkin, M. S., DeRose, E. F., Wall, M. J., Howell, E. E., and London, R. E. (2001) *Biochemistry 40*, 4242−4252.
44. Hribar, B., Southall, N. T., Vlachy, V., and Dill, K. A. (2002) *J. Am. Chem. Soc. 124*, 12302−12311.
45. Kao, Y.-H., Fitch, C. A., Bhattacharya, S., Sarkisian, C. J., Lecomte, J. T. J., and Garcia-Moreno, E. B. (2000) *Biophys. J. 79*, 1637−1654.
46. Courtenay, E. S., Capp, M. W., and Record, M. T. J. (2001) *Protein Sci. 10*, 2485−2497.
47. Magalhaes, A., Maigret, B., Hoflack, J., Gomes, J. N., and Scheraga, H. A. (1994) *J. Protein Chem. 13*, 195−215.
48. Zhu, Z.-Y., and Karlin, S. (1996) *Proc. Natl. Acad. Sci. U.S.A. 93*, 8350−8355.
49. Honig, B. (1995) *Science 268*, 1144−1149.
50. Koch, U., Biasiol, G., Brunetti, M., Fattori, D., Pallaoro, M., and Steinkuhler, C. (2001) *Biochemistry 40*, 631−640.
51. Radic, Z., Krichoff, P. D., Quinn, D., McCammon, A. W., and Taylor, P. (1997) *J. Biol. Chem. 272*, 23265−23277.

BI034643D